



Published in final edited form as:

Biochemistry. 2015 September 15; 54(36): 5589–5604. doi:10.1021/acs.biochem.5b00623.

Replication-Competent Influenza Virus and Respiratory Syncytial Virus Luciferase Reporter Strains Engineered for Co-Infections Identify Antiviral Compounds in Combination Screens

Dan Yan¹, Marco Weisshaar¹, Kristen Lamb¹, Hokyung K Chung², Michael Z Lin^{3,4}, and Richard K Plemper^{1,*}

¹Institute for Biomedical Sciences, Georgia State University, Atlanta, GA

²Department of Biology, Stanford University, Stanford, CA

³Department of Bioengineering, Stanford University, Stanford, CA

⁴Department of Pediatrics, Stanford University, Stanford, CA

Abstract

Myxoviruses such as influenza A virus (IAV) and respiratory syncytial virus (RSV) are major human pathogens, mandating the development of novel therapeutics. To establish a high-throughput screening protocol for the simultaneous identification of pathogen- and host-targeted hit candidates against either or both pathogens, we have attempted coinfection of cells with IAV and RSV. However, viral replication kinetics were incompatible, RSV signal window was low, and an IAV-driven minireplicon reporter assay used in initial screens narrowed the host cell range and restricted to single-cycle infections. To overcome these limitations, we developed an RSV strain carrying firefly luciferase fused to an innovative universal small-molecule assisted shut-off domain, which boosted assay signal window, and a hyperactive fusion protein that synchronized IAV and RSV reporter expression kinetics and suppresses the identification of RSV entry inhibitors sensitive to a recently reported RSV pan-resistance mechanism. Combined with a replication-competent recombinant IAV strain harboring nano-luciferase, the assay performed well on a human respiratory cell line and supports multi-cycle infections. Miniaturized to 384-well format, the protocol was validated through screening of a set of the NIH Clinical Collection (NCC) in quadruplicate. These test screens demonstrated favorable assay parameters and reproducibility. Application to a LOPAC library of bioactive compounds in a proof-of-concept campaign detected licensed anti-myxovirus therapeutics, ribavirin and the neuraminidase inhibitor zanamivir, and identified two unexpected RSV-specific hit candidates, Fenretinide and the opioid receptor antagonist BNTX-7. Hits were evaluated in direct and orthogonal dose-response counterscreens using a standard recRSV reporter strain expressing renilla luciferase.

Keywords

drug discovery; influenza virus; respiratory syncytial virus; recombinant viral reporter strains; high-throughput screening

*To whom correspondence should be addressed: Institute for Biomedical Sciences, Petit Science Center, Ste 712, Georgia State University, 100 Piedmont Av, Atlanta, GA 30303-3222, USA, rplemper@gsu.edu, phone: 404-413-3579.

Introduction

The myxovirus families include major human respiratory pathogens such as influenza virus, RSV, measles virus (MeV), and the highly pathogenic henipaviruses¹. Of these, RSV and the influenza viruses are pharmaceutically most relevant.

RSV, a member of the paramyxovirus family, is the leading cause of infant hospitalization due to viral infection in the United States and responsible for the majority of viral death among children below one year of age². Approximately 1% of the winter infant cohort (~125,000 patients) is hospitalized in the US with RSV disease annually^{2, 3}. Infants born prematurely, with bronchopulmonary dysplasia or a congenital heart defect are at highest risk of developing severe RSV disease⁴. While reinfection with RSV can occur throughout life⁵, RSV is life-threatening to the elderly and the immunocompromised⁶.

Clinical symptoms of human infection by major paramyxovirus pathogens such as MeV are dominated by host immunopathology⁷, closing the window for therapeutic intervention after the onset of symptoms⁸. In the case of RSV, however, several studies have challenged the paradigm that RSV pathogenesis is the result of host immunopathology alone. Higher viral loads were identified as a prediction of severe lower respiratory RSV infection in infants⁹ and RSV load on day three after hospitalization was associated with a requirement for intensive care and respiratory failure in children less than two years old¹⁰. These observations suggest that efficacious therapeutics given early to hospitalized children may improve downstream morbidity and reduce immunopathology, opening an opportunity for improved disease management. While RSV elicits innate and adaptive immune responses, the virus is poorly immunogenic overall and neutralizing antibody titers wane quickly post infection⁵, making vaccine development challenging despite extensive research. Immunoprophylaxis with the neutralizing antibody palivizumab is reserved for high-risk patients due to prohibitive costs¹¹ and ribavirin, although approved for RSV treatment, has little clinical benefit due to efficacy and toxicity issues¹².

IAV account for 3 to 5 million infections per year, representing the overall leading cause of human respiratory disease due to viral infection¹³. In the US alone, seasonal influenza alone is responsible for 20,000 to 40,000 deaths per year and poses a substantial economic burden due to decreased productivity and healthcare costs associated with hospitalization and/or treatment¹³. Morbidity and mortality associated with pandemic and emerging, highly pathogenic influenza strains can be substantially higher¹⁴⁻¹⁶.

The current seasonal influenza vaccines show efficacy in 70% of vaccinated adults but only 40% of the elderly^{1, 17-19}. Neuraminidase inhibitors are the predominant class of anti-influenza virus therapeutics and oseltamivir is still the primary drug stockpiled for pandemic preparedness. It is recommended for treatment of seasonal IAV H1N1, H3N2, and influenza B virus strains²⁰. However, efficacy in humans is moderate²¹ and is a subject of debate²²⁻²⁴. The issue is aggravated by the emergence of resistance to oseltamivir, which affects seasonal, pandemic and highly pathogenic avian influenza strains^{18, 19}.

The development of novel therapeutic against IAV and RSV infections is urgently needed to address the significant morbidity and mortality, the high socioeconomic toll, and the emergence of strains with preexisting resistance against available antivirals that we experience with these pathogens^{25, 26}. Host-targeted antivirals have experienced a renaissance in the last decade based on the promise of combining low frequencies of emerging viral resistance with a broadened antiviral indication spectrum²⁷⁻²⁹. However, the host-directed approach is inherently at a higher risk of inducing unacceptable side effects and efficacy can be compromised by alternative host pathways that may functionally replace the therapeutically targeted pathway *in vivo*^{30, 31}.

While there are tangible advantages associated with host-directed antivirals, narrowly designed drug discovery campaigns are inherently challenged by the risk of early stage failure due to a shallow candidate pool. In search of a resource-effective approach that simultaneously interrogates the full host-pathogen interactome for both pathogen-directed and host-directed hit candidates in a single well setting, we have recently described a dual myxovirus pathogen high throughput screening (HTS) assay³². Based on the hypothesis that the anticipated broadened indication spectrum of host-directed antivirals itself can be employed as the selector for hit candidates, we combined in this first implementation of the strategy an IAV isolate driving a firefly luciferase minigenome reporter with a recombinant MeV reporter strain expressing renilla luciferase. MeV, a paramyxovirus, was chosen as a replacement for RSV, since we found that fast IAV and slow RSV reporter expression kinetics were incompatible³². We demonstrated that ortho- and paramyxoviruses efficiently co-replicate, thus allowing the automated identification of orthomyxovirus-specific, paramyxovirus-specific, and broad-spectrum drug candidates in a robust assay format. Implementation of this dual-pathogen protocol in a proof-of-concept screen identified, amongst others, the pan-myxovirus blocker compound 09167, which acts by stimulating the expression of effector genes of host antiviral pathways³².

Despite this confirmation of general feasibility, the pilot screen also highlighted several limitations of the original assay: i) the IAV minireplicon reporter is resource-intensive, since it mandates reporter plasmid transfection and cryo-preservation of transfected cells prior to seeding into high-density assay plates; ii) expression of the minireplicon construct must be driven either by the T7 polymerase or RNA polymerase I, which restricts the conceivable host cell range to cell lines stably expressing T7 polymerase or lines with high intrinsic RNA Pol I activity, such as 293T cells³²; iii) poorly synchronized IAV and RSV reporter expression kinetics necessitated the use of a recombinant MeV reporter strain as a paramyxovirus surrogate, which excluded the identification of pathogen-directed RSV inhibitors. It was therefore the goal of the present study to develop and implement in a feasibility screen innovative myxovirus reporter strains that overcome these limitations and support direct drug screens with replication-competent IAV and RSV reporter strains in a robust HTS campaign.

Materials and Methods

Cell lines and transfections

Human carcinoma (HEp-2, ATCC CCL-23), human lung carcinoma (A549, ATCC CCL-185), human bronchial epithelial (BEAS-2B, ATCC CRL-9609), human embryonic kidney (293T, ATCC CRL-3216), and Madin Darby canine kidney (MDCK, ATCC CCL-34) cells were maintained at 37°C and 5% CO₂ in Dulbecco's modified Eagle's medium (DMEM) supplemented with 7.5% fetal bovine serum. Baby hamster kidney (BHK-21) cells stably expressing T7 polymerase (BSR-T7/5 cells)³³ were incubated at every third passage in the presence of 500 µg/ml G-418 (Geneticin). Lipofectamine 2000 (Invitrogen) was used for all transient transfection reactions.

Generation of recIAV reporter strains

Recombinant IAV/WSN/33 (H1N1) (IAV-WSN) strains were generated using the 8-plasmid IAV rescue system³⁴. Plasmids pHW12-PB1, pHW12-PB2, pHW12-PA, pHW12-NP, pHW12-HA, pHW12-NA, pHW12-M and pHW12-NS were kind gifts from David Steinhauer (Emory University). Recombinant IAV containing renilla and gaussia luciferase reporters in the NS1 and PB2 segments were generated as previously described^{35, 36}. recIAV-WSN harboring nano luciferase in the PB2 segment was constructed analogous to recIAV-WSN gaussia. Briefly, the PB2 3' packaging signal was inactivated through silent mutagenesis and a nano luciferase-encoding open reading frame (ORF) harboring a 3' KDEL-encoding endoplasmic reticulum retention signal fused to the mutant PB2 ORF through recombineering PCR. Nano and gaussia luciferase genes were amplified from plasmids pNL1.1CMV[Nluc/CMV] (Promega) and pTK-Gaussia (ThermoFisher), respectively. A 2A cleavage sequence from porcine teschovirus³⁷ was inserted between the PB2 and luciferase ORFs, and a copy of the original PB2 packaging signal inserted downstream of the coding cassette. All plasmids were sequence confirmed.

IAV recovery, amplification, and stability testing

All recIAV strains were recovered through rescue plasmid transfection into 293T cells and overlay of transfected cells onto MDCK cells after 28 hours of incubation. Recovered recombinants were amplified and released virions titered through plaque assay on MDCK cells. For genetic stability testing, recombinant virions were passaged consecutively four times and virus titers determined through plaque assays after each passage. In parallel, reporter titers were determined after each passage through 50% tissue culture infective dose (TCID₅₀) titration with bioluminescence as the readout, using a Synergy H1 (BioTek) multimode microplate reader equipped with substrate injectors.

Generation of recRSV reporter strains

Backbone for all recombinant RSV strains was a plasmid containing a full-length cDNA copy of a chimeric RSV-A2 genome, in which the F-encoding open reading frame was replaced with that of the line19 (L19) RSV isolate and an additional renilla luciferase ORF was added³⁸. The D489E substitution was introduced into L19 F through directed mutagenesis of a helper vector harboring a SacII/SalI fragment of the genome, followed by

transfer into the full-length plasmid and sequence confirmation, creating recRSV A2-L19F_{D489E}-renilla. Recombineering PCR was employed to add RSV intergenic junctions and flanking regions to firefly luciferase ORF, followed by substitution of a renilla luciferase-containing BstBI/AvrII fragment in recRSV A2-L19F_{D489E}-renilla with the equivalent fragment harboring firefly luciferase. To generate the fireSMASH ORF, the SMASH tag³⁹ was fused in frame to the 3' end of the firefly luciferase ORF through recombineering PCR, followed by addition of the RSV flanking regions and BstBI/AvrII transfer into the full length cDNA genome copy as before. recRSV were recovered through co-transfection with RSV L, N, P, and M2-encoding helper plasmids into BSR-T7/5 cells as previously described³⁸, and subjected to RT-PCR and cDNA sequencing.

RSV recovery, amplification, and stability testing

recRSV stocks were grown on HEp-2 cells inoculated at a multiplicity of infection (MOI) of 0.01 pfu/cell. Infected cells were kept for 16 hours at 37°C, followed by incubation at 32°C for five to seven days. Cell-associated progeny virus was released through one freeze/thaw cycle and titers determined by TCID₅₀ titration on HEp-2 cells. For genetic stability testing of the SMASH tagged virus, recovered recRSV A2-L19F-fireSMASH virions were consecutively passaged five times on HEp-2 cells. Progeny virions of the second and fifth passage were incubated in the presence or absence of 3 μM asunaprevir (ASV) and infected cell lysates subjected to SDS-PAGE and immunoblotting.

SDS-PAGE and antibodies

Infected cells (6×10^5 per well in a 6-well plate format) were lysed 40 hours post-infection in RIPA buffer (1% sodium deoxycholate, 1% NP-40, 150 mM NaCl, 50 mM Tris-Cl, pH 7.2, 10 mM EDTA, 50 mM sodium fluoride, protease inhibitors [Roche], 1 mM phenylmethylsulfonyl fluoride), subjected to clearance centrifugation (20,000×g for 30 minutes at 4°C) and cleared lysates diluted with UREA buffer (200 mM Tris, pH 6.8; 8 M urea; 5% sodium dodecyl sulfate (SDS); 0.1 mM EDTA; 0.03% bromophenolblue; 1.5% dithiothreitol) at a 1:2-ratio. Denatured (30 minutes at 50°C) lysates were fractionated through gel electrophoresis on 10% Tris/Glycine gels, transferred to polyvinylidene difluoride (PVDF) membranes (GE Healthcare), and protein material detected through decoration with specific antibodies directed against firefly luciferase (PA5-32209, ThermoFisher) or glyceraldehyde-3-phosphate dehydrogenase (anti-GAPDH, Calbiochem). Immunoblots were developed using mouse IgG light chain-specific HRP-conjugated secondary antibodies (Jackson) and a ChemiDoc digital imaging system (Bio-Rad).

Purification of virus stocks

Two alternative strategies were explored to remove contaminating luciferase proteins from virus stocks. Progeny virions in culture supernatants (IAV stocks) or released through one freeze/thaw cycle from infected cells (RSV stocks) were cleared (4,000×g for 20 minutes at 4°C), then pelleted (60,000×g for 30 minutes at 4°C). Pelleted material was resuspended in TNE buffer (50 mM Tris/Cl pH 7.2, 10 mM EDTA) and purified through a 20/60% one-step sucrose gradient in TNE buffer (100,000×g for 90 minutes at 4°C). Virions were harvested from the gradient intersection. Alternatively, cleared RSV stocks were purified and polished through size exclusion and binding chromatography by passaging through dual functionality

Capto Core 700 resin (GE Healthcare) using an ÄKTA avant chromatography system (GE Healthcare). After purification through either method, virus stocks were stored in aliquots at -80°C .

Reporter expression profiles

Cells (1.5×10^4 per well in a 96-well plate format) were infected with purified virus stocks at different MOIs as specified or co-infected. At the specified time points, cells were lysed *in situ* with 50 μl Glo-lysis buffer (Promega) for five minutes at 37°C and samples transferred into solid white 96-well plates. Lysates were kept frozen until the time course was completed, then equilibrated to ambient temperature simultaneously and relative luciferase activities determined using the Synergy H1 reader and injectors to add renilla-Glo, bright-Glo or dual-Glo substrates (all Promega), respectively (lag time before reading three minutes for each well). Values are expressed for each reporter strain relative to the highest reading recorded for this strain, and represent averages of at least three independent repeats.

Compounds

All compounds were dissolved in DMSO to 10 mM concentration and stored at -80°C . The MScreen software package⁴⁰ was used for electronic compound management, HTS data storage and data analysis. Compounds of the NIH Clinical Collection (NCC) were received from the NIH Small Molecule Repository in 96-well plates, inventoried in MScreen, and reformatted into barcoded 384-well daughter plates using a Nimbus liquid handler (Hamilton Robotics) with multichannel pipetting head. In addition, known anti-myxovirus bioactives that we have identified in previous drug discovery campaigns were included in empty wells in the NCC daughter plates. Thirty-two wells on each 384-well plate received compound JMN3-003³⁰ for positive control, and another 32 wells received volume equivalents of vehicle (DMSO) only. Asunaprevir (ASV) was obtained from Santa Cruz Biotechnology. When included, ASV was added at the time of virus infection.

Assay validation in 96-well format

BEAS-2B cells (2×10^4 /well, seeded in 40 μl in white wall/clear bottom 96-well plates) were treated manually (1 μl /well) with a set of known bioactives (diluted in growth media to 5% DMSO, final concentration as specified), then infected or co-infected with 10 μl of the IAV and RSV reporter viruses at different MOIs as specified. Final DMSO concentrations were 0.1%, at which no vehicle-induced cytotoxic effect was detected. After a 40-hour incubation period at 37°C , luciferase substrates (25 μl /well) were injected as before directly into the assay plates and relative bioluminescence intensities determined. Each compound was assessed in five replicates. For quantitative assay validation, Z' values⁴¹ were calculated according to the formula $Z' = 1 - (3SD_{(C)} + 3SD_{(B)}) / (\text{Mean}_{(C)} - \text{Mean}_{(B)})$, with C = control and B = background.

Automated HTS protocol in 384-well plate format

BEAS-2B cells (8×10^3 /well) were injected in 30 μl /well into barcoded white wall/clear bottom 384-well plates using a MultiFlo automated dispenser (BioTek) equipped with dual 10- μl peristaltic pump manifolds, collected (150 \times g for 90 seconds at 25°C), and incubated

for five hours at 37°C and 5% CO₂. Compound was added to a final concentration of 5 μM (20 nl/well) using a high-density pin tool (V&P Scientific) attached to the pipetting head of the Nimbus liquid handler, followed by co-infection with recRSV A2-L19F_{D489E}-fireSMASH (MOI = 0.1) and recIAV WSN-NanoLuc (MOI = 0.02) in 10 μl/well using the MultiFlo dispenser unit, spin collection (150×g for 90 seconds at 25°C), and incubation for 40 hours at 37°C and 5% CO₂. Final vehicle (DMSO) concentration was 0.05%. Barcodes of source and assay plates were automatically detected and recorded by the Nimbus unit at the time of stamping. Using a stacker unit with integrated barcode reader (Biotek) attached to the H1 synergy plate reader, plates were automatically loaded, dual-Glo substrates (15 μl/well each) injected, and bioluminescence recorded after a three minute lag time for each well and substrate. Readouts were automatically saved by plate barcode. For manual calculation of Z' values, luciferase activities in positive and vehicle wells were processed as detailed above.

Dose-response counterscreens

Two-fold serial dilutions of hit candidates were prepared in 384-well plates in three replicates each using the Nimbus liquid handler. BEAS-2B cells (8×10^3 /well) were then plated as before, serial dilutions transferred using the pin-tool, and cells infected with recRSV A2-L19F_{D489E}-fireSMASH (MOI = 0.1), recRSV A2-L19F-renilla (MOI = 0.1), or recIAV WSN-NanoLuc (MOI = 0.02), or left uninfected for cell viability assessment. Reporter signals were recorded as outlined above. To determine cell viability, PrestoBlue substrate (life technologies) was added after 40-hour incubation of cells at 37°C (5 μl/well) and top-read fluorescence (excitation 560 nm; emission 590 nm; instrument gain 85) recorded after 45 minutes of incubation at 37°C using the H1 synergy plate reader. Four-parameter variable slope regression modeling was applied to determine 50% active (EC₅₀) and toxic (CC₅₀) concentrations.

Data normalization and analysis

The MScreen package was employed for automated data analysis. Plate reader raw data files together with source and assay plate barcode maps generated by the Nimbus system were directly imported into the package, and Z' values automatically calculated based on the designated control wells. Since the NCC plates contained a high density of known bioactives, the normalized percent inhibition method was applied for data analysis. Normalized relative inhibition values were calculated for each compound by subtracting each value from the average of the plate vehicle controls, followed by dividing the results by the difference between the means of plate vehicle and positive controls. Hits candidates were defined as compounds showing 75% inhibition of normalized signal intensity against either or both viral targets. For analysis of replicate plates, the cellHTS2 package⁴² was employed to calculate percent inhibition as described above, followed by scaling of plates by dividing the normalized value of each well by the median absolute deviation of the plate. Results are given as Z scores, positive Z scores reflecting more potent inhibition. The dynamic range was calculated for each plate as the ratio between the geometric means of the positive and negative controls. The SciFinder database package (American Chemical Society) was used to query chemical databases with hit candidate structures to evaluate known bioactivities.

Statistical analysis

The Excel and Prism 6 (GraphPad) software packages were used for data analysis. Statistical significance of differences between two sample groups were assessed by unpaired two-tailed *t* tests (two sample groups; Excel), or two-way analysis of variance (ANOVA; Prism 6) in combination with Tukey's multiple comparison post-tests (multiple sample groups) as specified in the figure legends. Experimental uncertainties are identified by error bars, representing standard deviations (*SD*).

Results

Different versions of replication-competent IAV strains encoding luciferase reporters were described recently^{35, 43}. Of these, a recombinant IAV-PR8 harboring a *Gaussia* open reading frame in the PB2 genome segment reportedly replicated efficiently, was genetically stable, and showed high luciferase activity levels³⁵.

Generation of a replication-competent IAV-WSN PB2-NanoLuc reporter strain

Most laboratory IAV strains require the addition of exogenous trypsin for proteolytic maturation of the HA protein for priming of the viral entry machinery. To gain independence of trypsin activation in all screening plates, we generated the analogous PB2-*Gaussia* recombinant in the trypsin-independent IAV-WSN genetic background (figure 1A;⁴⁴). The resulting recIAV-WSN *Gaussia* showed efficient replication and reporter expression in the absence of exogenous trypsin (figure 1B). However, the signal window of *Gaussia* remained below 10 (figure 1C). Towards extending the assay range, we substituted *Gaussia* luciferase for the recently developed Nano luciferase (NanoLuc, figure 1A), which uses the same basic substrate chemistry as *Gaussia* and *Renilla* luciferases but combines a small protein size with high signal intensities. Recovered recIAV-WSN NanoLuc indeed returned an over six-fold improved signal window and showed superior absolute luciferase signal intensities compared to recIAV-WSN *Gaussia* (figures 1C and D). *Z'* values in either case far exceeded 0.5, suggesting that the assay is suitable for automation. Serial passaging of this recombinant confirmed equivalent genetic stability of recIAV-WSN *Gaussia* and recIAV-WSN NanoLuc. By comparison, luciferase activity rapidly disappeared when a recIAV-WSN NS-*Gaussia* was subjected to passaging, which harbors the luciferase open reading frame in the NS genome segment (figure 1E). The design of this recombinant followed the strategy outlined in a recent report³⁶.

An IAV-compatible recombinant RSV-firefly reporter strain

In the original evaluation of a dual-myxovirus HTS protocol, we found that IAV and MeV-based reporter expression overlapped, whereas the original recRSV-L19F-*renilla* reporter strain showed a substantial delay in luciferase expression over a range of different inoculum multiplicities of infection (MOIs). When comparing RSV and MeV in cell culture, most notably is the divergence in cell-to-cell fusion (syncytia formation) after infection, which represents the hallmark of MeV cytopathicity but is much less pronounced in the case of RSV. We therefore hypothesized that the lower rate of lateral RSV spread may cause the slower reporter expression kinetics, and asked whether a hyperfusogenic RSV variant would

alleviate the problem. We have previously generated an RSV recombinant with a D to E substitution of fusion (F) protein residue 489 that renders it hyperfusogenic ⁴⁵.

To test the effect of hyperfusogenicity on reporter expression kinetics, we generated a recRSV-L19F_{D489E}-firefly strain (figure 2A) analogous to the previously described recRSV-L19F-renilla, since firefly and nano luciferase activities are based on distinct substrate chemistry and can be independently quantified. Independent of the nature of the luciferase reporter included, time to peak reporter activity of F_{D489E} mutant strains was less than half that of a strain harboring standard F (figure 2B). These results suggest that the hyperfusogenic recRSV-L19F_{D489E}-firefly strain should be suitable for co-infection screens with recIAV WSN-NanoLuc. When attempting to purify recRSV-L19F_{D489E}-firefly preparations from contaminating firefly protein that was synthesized during stock growth, however, we noted that both gradient ultracentrifugation and layered bead chromatography purification strategies successfully reduced renilla luciferase contaminations, but by comparison remained inefficient against firefly luciferase (figure 2C). As a consequence, the signal window of assays based on the recRSV-L19F_{D489E}-firefly strain was approximately 8-fold lower than that achievable with recRSV-L19F_{D489E}-renilla (figure 2D), excluding its use in high-density HTS applications.

SMASH technology to eliminate contaminating firefly protein

In search of an innovative approach to suppress the build-up of contaminating firefly protein during growth of virus stocks, we explored the use of small molecule-assisted shutoff (SMASH) technology for induced protein degradation that we have recently developed ³⁹. Unlike other systems designed to induce protein turnover, only SMASH functions as a single-chain system and in the stabilized state returns near-native proteins. Added as a genetic tag, SMASH consists of a hepatitis C virus-derived NS3 protease flanked by a strong degron domain inducing proteasomal degradation. An NS3 protease site is positioned at the intersection of the SMASH tag and the target protein (figure 3A). Under normal conditions, NS3 autoproteolysis separates the tag, returning the near-native target protein. In the presence of a strong NS3 inhibitor such as the clinical candidate ASV ⁴⁶, however, autoproteolysis is blocked and the degron domain induces rapid degradation of the tag and affixed target protein.

We added a SMASH tag to the firefly open reading frame and successfully recovered the corresponding recRSV-L19F_{D489E}-fireSMASH recombinant. Immunoblotting with antibodies directed against firefly luciferase confirmed efficient degradation of the tagged protein after incubation in the presence of ASV, while steady state levels closely matched those of untagged firefly luciferase in the absence of the drug (figure 3B). As expected, ASV had no effect on progeny virus titers (figure 3C) and the SMASH tag remained stable over multiple passages of this virus strain (figure 3D). However, growth of recRSV-L19F_{D489E}-fireSMASH in the presence of ASV reduced firefly luciferase activity by approximately 90% (figure 3E), which paved the path for improved assay performance (figure 3F) and an over 23-fold increased signal window of recRSV-L19F_{D489E}-fireSMASH compared to recRSV-L19F_{D489E}-firefly (figure 3G). These results suggest that recIAV WSN-NanoLuc and

recRSV-L19F_{D489E}-fireSMASH may represent a suitable pair for dual-pathogen drug discovery campaigns.

Co-infection conditions

To establish suitable assay conditions, we first independently infected three human respiratory cell lines, HEp2, BEAS-2B, and A549, with recRSV-L19F_{D489E}-fireSMASH and recIAV WSN-NanoLuc at different multiplicities of infection and measured relative luciferase activities at 40 hours post-infection to test for host cell preference of the reporter strains. At each MOI, RSV-based reporter expression was reduced in A549 cells by over 90% compared to each of the other two cell lines (figure 4A), and a comparable reduction was observed with IAV-based NanoLuc expression in HEp2 cells (figure 4B).

We therefore selected BEAS-2B cells as best suited for RSV/IAV co-infection experiments and generated reporter expression profiles after infection with either virus individually (figures 4C and D) or in combination (figure 4E). Peak luciferase activities (RLUs 80% of max) overlapped in an approximately 7-hour time window (37-44 hours post-infection) when cells were co-infected with recRSV-L19F_{D489E}-fireSMASH at an MOI of 0.1 and recIAV WSN-NanoLuc at an MOI of 0.02. All subsequent experiments followed these assay conditions, and reporter signals were measured 38-42 hours post-infection.

Assay miniaturization and validation

Towards validating the assay for screening campaigns, we initially applied the protocol in 96-well plate format to a panel of known bioactives with discrete anti-myxovirus activity and cytotoxic compounds for comparison (figure 5A). Relative inhibition was calculated through normalization of raw data for control wells that received vehicle (DMSO) only. In all cases, known myxovirus inhibitors with different antiviral profiles were correctly identified, and Z' values (figure 5B) exceeded 0.5, defining a robust assay⁴⁷. The previously characterized RSV fusion blockers GPAR3710 and BMS-433771^{45, 48} did not emerge as hits, confirming our hypothesis that the use of the pan-resistant RSV-F_{D489E} mutant will reliably suppress the discovery of additional, undesirable RSV entry inhibitors that are also sensitive to the pan-resistance escape mechanism that we have recently described⁴⁵.

Based on this proof-of-concept data, we miniaturized the assay to 384-well plate format and screened a 2-plate pilot set of the National Compound Collection (NCC) in quadruplicate to quantify assay suitability for automated hit discovery and determine plate-to-plate and day-to-day reproducibility. In addition, we added previously identified broad-spectrum myxovirus inhibitors³⁰ to the NCC set for reference. Executed under HTS conditions, this validation campaign returned robust Z' values exceeding 0.5 and a signal window greater than 50 (RSV) and 20 (IAV), respectively (figure 5B).

Of the NCC test library, 11 hit candidates were identified that inhibited primary reporter activities by 75% or greater of either or both target viruses (table 1). The majority of these hit candidates were previously associated with diverse antiviral and/or cytotoxic activities. Graphic representation of all assay validation replicates in Z -score profiles revealed that the dual myxovirus protocol shows high plate-to-plate reproducibility (figure 5C). Plotting of

individual z-scores of each replicate as a function of mean %-inhibition values for each compound and viral target furthermore revealed a strong correlation between normalized scores and effect sizes for all hit candidates (figure 5D).

Test screen of a 1280-compound library

For proof-of-concept of hit identification under single-replicate screening conditions, we applied the validated assay to the LOPAC1280 library of pharmacologically active compounds (figure 6A). This campaign yielded 24 primary hit candidates (1.875% hit rate). Positives included, amongst others, known anti-influenza virus and anti-RSV inhibitors (Zanamivir and Ribavirin), protein biosynthesis blockers (i.e. Emetine), and DNA/RNA synthesis inhibitors (i.e. PMEG and Idarubicin) (table 2). Of note, Zanamivir, Ribavirin, and Amantidine were the only antiviral drugs in this library licensed for the treatment of IAV and/or RSV infections. Since the recIAV-WSN strain used for screening is resistant against the M2 channel blocker amantidine, the assay correctly identified all licensed therapeutics with anti-myxovirus indication.

All compounds were picked (table 2 and supplement information table S1) and subjected to cytotoxicity testing. Only candidates that reduced cell viability by less than 50% at twice the screening concentration (10 μ M) were admitted to automated dose-response testing (14 compounds; table 2) against the primary screening strains. Interference with luciferase reporter or the NS3 protease activity of the SMASh tag was addressed in parallel by testing against a standard recRSV A2-L19F reporter strain lacking the F_{D489E} resistance mutations and expressing renilla luciferase that does not share substrate chemistry with firefly luciferase³⁸. Compound interference with nano-Luciferase is addressed by testing against cells transiently transfected with a nano-luciferase expression plasmid in our confirmation pipeline, but we did not implement this counterscreen in this exercise since only the licensed influenza drug Zanamivir selectively inhibited the IAV reporter. Whenever possible, 50% active and cytotoxic concentrations of the selected hit candidates were calculated for all assay targets through four-parameter variable slope regression modeling (table 2).

Triptolide of the NCC test-set originally demonstrated preferential activity against the IAV reporter strain and was likewise selected for dose-response testing and sourced. Of the resulting 15 candidates, five showed only a marginal inhibitory effect against the primary screening strains or were inactive, and Triptolide returned an SI (CC₅₀/EC₅₀) value below two at dose-response testing. The remaining nine viable primary hits either blocked preferentially RSV (2 compounds) or IAV (2 compounds) reporter expression, or suppressed both reporter strains (5 compounds) (figure 6B).

First inspection reveals that these confirmed hits can be classified into three distinct groups: i) licensed antiviral therapeutics such as Zanamivir and Ribavirin; ii) compounds with documented broad-spectrum antiviral activity such as the nucleoside analog Gemcitabine^{49, 50} and inhibitors of the purine or pyrimidine biosynthesis pathways such as Aminopterin and Brequinar, respectively^{51, 52}; and iii) compounds not yet extensively associated with anti-ortho- or paramyxovirus activity (Fenretinide, BNTX-7, and PMEG hydrate (table 2)). Of these, Fenretinide and BNTX-7 selectively inhibited RSV, while the IAV reporter strain was unaffected at the highest concentration tested. PMEG hydrate

blocked both reporter strains, although potency against RSV was approximately 2-fold higher than against IAV.

These results demonstrate that the new generations of recombinant RSV and IAV reporter strains generated in this study can be combined in a robust screening protocol miniaturized to 384-well format. The assay successfully identifies licensed therapeutics and compounds with known anti-myxovirus activity. A set of RSV inhibitors merits further mechanistic evaluation.

Discussion

In this study, we have developed and validated a dual pathogen myxovirus HTS protocol that uses innovative protein engineering technology for the simultaneous discovery of pathogen-specific and broad spectrum hit candidates (figure 7). There are several major advantages of this protocol over traditional single pathogen screens and a first generation co-infection screen that we have reported earlier³²: i) compared to consecutive screening of a library against individual viral targets, the dual pathogen protocol using replication-competent recombinant viruses shows superior cost and resource effectiveness; ii) the screening agents used in the new approach, IAV and RSV, are clinically the most significant members of the myxovirus families; iii) in addition to identifying broad-spectrum blockers, the dual readout strategy creates a bona fide “internal standard” for each well, excluding cytotoxic and undesirable promiscuous compounds effectively from the pool of virus-specific hit candidates at the stage of primary screening; iv) the new assay is not systemically restricted in host cell range, but applicable to all cell lines permissive for IAV and RSV replication including human respiratory epithelial cells; and v), the current assay is suitable for multiple cycle infections, providing flexibility in the choice of inoculum MOI and allowing the interrogation of all stages of the viral live cycle.

Three generations of HTS reporter assays were developed in recent years for the identification of novel influenza virus inhibitors⁵³. First generation assays employed influenza virus-activated reporters, second generation systems are based on recombinant virions in which one of the viral open reading frames is substituted for a reporter gene, and third generation influenza virus reporter strains harbor the reporter as additional genetic information in one of the genome segments. Compared to traditional cell-based anti-influenza virus HTS screens that in the majority of cases simply monitor virus-induced cytotoxicity, common advantages to these reporter assays are the quantitative readout, the possibility for assay miniaturization beyond 96-well plate scale, and the higher accuracy of hit identification.

However, first generation assays require the labor- and resource-intensive preparation of target cell populations and only support single cycle infections. Both first and second generation assays are restricted by a narrow range of suitable target cell lines. By contrast, third generation influenza virus reporter assays combine high signal intensities with broad target cell flexibility. We therefore explored this strategy and found that the recently developed nano luciferase technology is particularly suitable for influenza reporter virus HTS applications due to small size and superior signal intensities, which translate into

robust assay parameters. Naturally, primary screening hits blocking the recIAV WSN-NanoLuc reporter strain must be counterscreened against a panel of currently circulating IAV strains of different genotypes to assess the full anti-IAV indication spectrum.

Our study spotlights that the introduction of the hyperfusogenic F_{D489E} mutation⁴⁵ into the RSV reporter strain accelerates the luciferase expression kinetics to a level that we previously observed only with MeV reporter strains³². Although MeV and RSV represent distinct paramyxovirus subfamilies, there is little reason to assume that the difference in reporter expression kinetics between RSV and MeV strains is due to substantially faster entry of MeV or slower gene expression of RSV compared to MeV. Our results rather indicate that the enhanced cell-to-cell fusion activity of the mutant RSV reporter strain and, thus, accelerated lateral spread through the cell monolayer⁴⁵, altered the reporter expression profile.

We have previously reported that the F_{D489E} mutation causes RSV pan-resistance against all known and characterized small-molecule RSV entry inhibitors, including those currently considered for clinical use⁵⁴⁻⁵⁶. The advantage of engineering the F_{D489E} substitution into the screening strain is therefore two-fold; firstly, hyperfusogenicity contributes to synchronizing IAV and RSV reporter expression profiles and, secondly, the mutation should efficiently suppress the discovery of additional RSV entry inhibitors that are likewise sensitive to the pan-resistance mechanism and have therefore little clinical potential. Consistent with this hypothesis, known RSV entry inhibitors that were spiked into the proof-of-concept screening library did not emerge as hit candidates in our assay validation screens.

Fluorescent recombinant RSV reporter strains were generated over a decade ago⁵⁷, but we only recently pioneered the application of luciferase reporter technology to the RSV system through the recovery of a recRSV A2-L19F-renilla reporter strain³⁸. Since *gaussia*, *renilla* and *nano luciferase* depend on the same substrate chemistry and the small *nano luciferase* ORF was most suitable for stable incorporation into a recombinant influenza virus strain, co-infection screening demanded the development of an RSV firefly reporter strain for combination with recIAV WSN-NanoLuc. Virus recovery was straight-forward, but high levels of contaminating firefly luciferase protein in virus stocks despite extensive purification of virus preparations prohibited assay miniaturization due to unacceptably low S/B ratios.

Remarkably, this problem did not surface in earlier work using the recRSV A2-L19F-*renilla* reporter³². Two explanations for the variation in purification success are conceivable; firefly but not *renilla luciferase* may nonspecifically absorb to RSV particles, or firefly luciferase may be incorporated efficiently into budding RSV virions. Either scenario would render the protein inaccessible to purification strategies designed to preserve the infectivity of the virus stock.

A variety of different approaches were developed to control protein steady state levels *in cellulo*. However, only the very recently pioneered SMASH technology operates as a single-chain system and returns the stabilized protein in its near-native state³⁹. Repeated passaging of the RSV recombinant harboring a fireSMASH open reading frame furthermore confirmed

that the tag is genetically stable in the RSV background. These features make the technology uniquely suitable for applications in recombinant virions and allow, for instance, a controlled shut-off of virus replication *in vitro* and *in vivo*³⁹. Applied to reporter viruses for HTS, SMASh provides an effective strategy to remove purification-resistant reporter proteins from virus stocks.

Test screening of the LOPAC1208 library in 384-well format using the fully validated assay correctly identified licensed antiviral therapeutics present in the library. In addition, Gemcitabine reportedly has antiretroviral and anti-influenza virus activity^{49, 50}, and compound blocking purine or pyrimidine biosynthesis were recognized in several previous drug screens as broad-spectrum antivirals^{30, 58, 59}. Taken together, the hits in groups (i) and (ii) that emerged from our assay are therefore fully consistent with known antiviral profiles, generating confidence in the accuracy of hit discovery by the protocol.

Of the other confirmed hits, Fenretinide and BNTX-7 selectively blocked RSV in our assay. Fenretinide is a synthetic retinoid derivative that was developed with anti-cancer and anti-cystic fibrosis endpoints⁶⁰. The compound also suppresses HIV infection, which was originally attributed to enhanced viral endocytosis⁶¹. However, a recent study demonstrating strong anti-Dengue virus activity suggested upregulation of the host cell unfolded protein response pathway as an alternative mechanism of activity⁶². BNTX-7 is a selective opioid delta receptor antagonist⁶³. Highly differential activity against RSV and IAV in our dose-response counterscreens excludes high cytotoxicity as the underlying cause of RSV inhibition, and comparable potency against both RSV A2-L19F-renilla and RSV A2-L19F_{D489E}-fireSMASh with distinct reporter technology argues against reporter interference. Opioid receptors are present on epithelial cells of the oral/respiratory tract⁶⁴. Remarkably, altered opioid receptor signaling was found to correlate with disease severity in human RSV infection and a mouse model⁶⁵, underscoring that a mechanistic evaluation of the role of opioid receptor signaling in RSV replication may uncover novel druggable targets. An assessment of the broader paramyxovirus indication spectrum of Fenretinide and BNTX-7 and a characterization of the underlying mechanism for selective RSV inhibition are currently underway.

PMEG hydrate blocked both IAV and RSV reporter strains. The compound is an acyclic nucleotide analog that results in DNA chain termination after conversion to the active diphosphate PMEGpp and incorporation⁶⁶. Prodrugs of PMEG such as GS-9191 are developed for the topical treatment of human papillomavirus infection⁶⁷. A second prodrug analog, GS-9219, acts antineoplastic in dogs with non-Hodgkin's lymphoma⁶⁸, but an unacceptable safety profile halted a human trial.

Whereas the dual pathogen approach inherently reduces the frequency of undesirable compounds from the pool of virus-specific hits, broad-spectrum candidates must be expected to include a substantial portion of cytotoxic or promiscuous entries³². In our test screen, more than half of the hit candidates blocking both reporter strains revealed cytotoxicity exceeding our cut-off value for follow-up counterscreens, highlighting that a wide antiviral indication spectrum is often penalized by linked to acute or chronic cytotoxicity.

Of the reporter virus-specific hits, compounds may be acting through reporter interference or, in the case of recRSV A2-L19F_{D489E}-fireSMASh, inhibition of the HCV-derived NS3 protease. Traditional virus yield-based secondary screens are suitable to address assay interference and NS3 protease blockage, but are labor and resource intensive. Having generated a diverse panel of myxovirus reporter strains harboring distinct luciferases³², we demonstrate the feasibility of a rapid automated counterscreening strategy that examines hit candidate activity against a luciferase reporter with distinct substrate chemistry. In the case of recRSV A2-L19F_{D489E}-fireSMASh, this approach also addresses any NS3 protease liability, since the fireSMASh was replaced by recRSV A2-L19F_{D489E}-renilla. We predict that the newly developed technologies and screening strategies reported here are applicable to a range of clinically-relevant viral targets and will prove effective in rapidly focusing developmental efforts on viable hit candidates.

Supplementary Material

Refer to Web version on PubMed Central for supplementary material.

Acknowledgements

We are grateful to D. Steinhauer for kindly providing the IAV-WSN rescue system, R. Cox for help with computer artwork, Y. Hu for technical assistance, R.T. Jacob for IT assistance, M. Ndungu and M.T. Saindane for chemical synthesis, M.L. Moore for providing the RSV reverse genetics system, and A.L. Hammond for critical reading of the manuscript. The MScreen software package was kindly provided by the Center for Chemical Genomics of the University of Michigan under a license agreement by the University of Michigan Office of Technology Transfer, JChem was used for structure database management, search and prediction (JChem 6.2, 2014, ChemAxon (<http://www.chemaxon.com>)), and Marvin was employed for drawing, displaying and characterizing chemical structures, substructures and reactions (Marvin 14.9.22.0, 2014, ChemAxon (<http://www.chemaxon.com>)).

Funding Sources

This work was supported, in part, by Public Health Service Grants AI071002, AI119196, and HD079327 from the NIH/NIAID and NIH/NICHD (to R.K.P.).

References

- [1]. Stiver G. The treatment of influenza with antiviral drugs. *Cmaj*. 2003; 168:49–56. [PubMed: 12515786]
- [2]. Thompson WW, Shay DK, Weintraub E, Brammer L, Cox N, Anderson LJ, Fukuda K. Mortality associated with influenza and respiratory syncytial virus in the United States. *JAMA*. 2003; 289:179–186. [PubMed: 12517228]
- [3]. Hall CB. Respiratory syncytial virus and parainfluenza virus. *The New England journal of medicine*. 2001; 344:1917–1928. [PubMed: 11419430]
- [4]. Mahadevia PJ, Masaquel AS, Polak MJ, Weiner LB. Cost utility of palivizumab prophylaxis among pre-term infants in the United States: a national policy perspective. *J Med Econ*. 2012; 15:987–996. [PubMed: 22574798]
- [5]. Collins, PL.; Crowe, JE, Jr.. Respiratory Syncytial Virus and Metapneumoviruses. In: Knipe, DM.; Howley, PM., editors. *Fields Virology*. 5. Lippincott, Williams, & Wilkins; Philadelphia: 2007. p. 1601-1645.
- [6]. Elliot AJ, Fleming DM. Influenza and respiratory syncytial virus in the elderly. *Expert review of vaccines*. 2008; 7:249–258. [PubMed: 18324893]
- [7]. de Vries RD, Mesman AW, Geijtenbeek TB, Duprex WP, de Swart RL. The pathogenesis of measles. *Curr Opin Virol*. 2012; 2:248–255. [PubMed: 22483507]

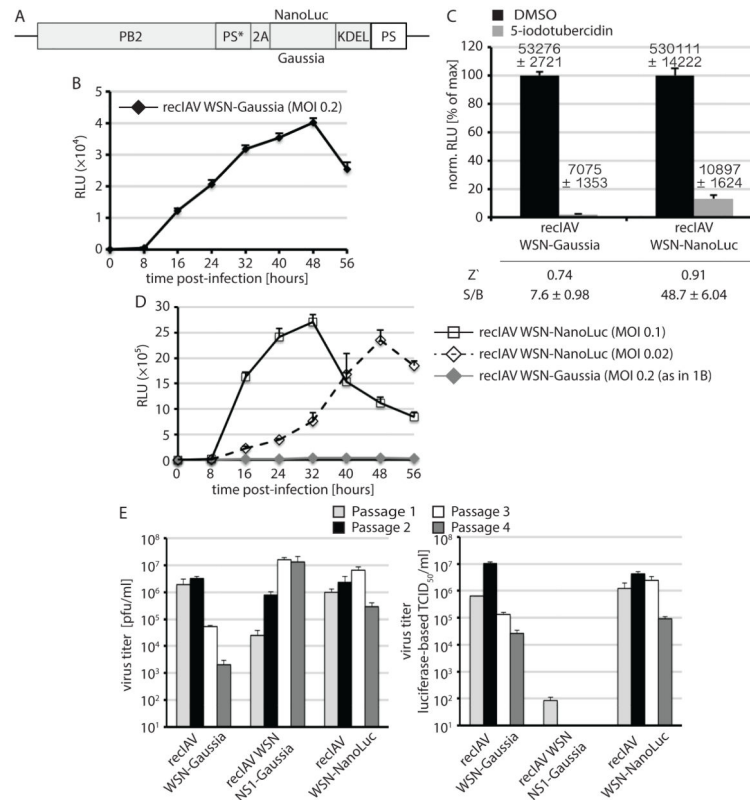
- [8]. Plemper RK, Hammond AL. Synergizing vaccinations with therapeutics for measles eradication. *Expert opinion on drug discovery*. 2014; 9:201–214. [PubMed: 24303998]
- [9]. DeVincenzo JP, El Saleeby CM, Bush AJ. Respiratory syncytial virus load predicts disease severity in previously healthy infants. *J Infect Dis*. 2005; 191:1861–1868. [PubMed: 15871119]
- [10]. El Saleeby CM, Bush AJ, Harrison LM, Aitken JA, Devincenzo JP. Respiratory syncytial virus load, viral dynamics, and disease severity in previously healthy naturally infected children. *J Infect Dis*. 2011; 204:996–1002. [PubMed: 21881113]
- [11]. Weiner LB, Masaquel AS, Polak MJ, Mahadevia PJ. Cost-effectiveness analysis of palivizumab among pre-term infant populations covered by Medicaid in the United States. *J Med Econ*. 2012; 15:997–1018. [PubMed: 22435648]
- [12]. Hall CB, Granoff DM, Gromisch DS, Halsey NA, Kohl S, Marcuse EK, Marks MI, Nankervis GA, Pickering LK, Scott GB, Steele RW, Yogev R, Peter G, Bart KJ, Broome C, Hardegree MC, Jacobs RF, Macdonald NE, Orenstein WA, Rabinovich G. Use of Ribavirin in the Treatment of Respiratory Syncytial Virus-Infection. *Pediatrics*. 1993; 92:501–504. [PubMed: 8361820]
- [13]. Beigel J, Bray M. Current and future antiviral therapy of severe seasonal and avian influenza. *Antiviral Res*. 2008; 78:91–102. [PubMed: 18328578]
- [14]. Gatherer D. The 2009 H1N1 influenza outbreak in its historical context. *J Clin Virol*. 2009; 45:174–178. [PubMed: 19540156]
- [15]. Li Q, Zhou L, Zhou M, Chen Z, Li F, Wu H, Xiang N, Chen E, Tang F, Wang D, Meng L, Hong Z, Tu W, Cao Y, Li L, Ding F, Liu B, Wang M, Xie R, Gao R, Li X, Bai T, Zou S, He J, Hu J, Xu Y, Chai C, Wang S, Gao Y, Jin L, Zhang Y, Luo H, Yu H, He J, Li Q, Wang X, Gao L, Pang X, Liu G, Yan Y, Yuan H, Shu Y, Yang W, Wang Y, Wu F, Uyeki TM, Feng Z. Epidemiology of human infections with avian influenza A(H7N9) virus in China. *The New England journal of medicine*. 2014; 370:520–532. [PubMed: 23614499]
- [16]. Taubenberger JK, Morens DM. 1918 Influenza: the mother of all pandemics. *Emerg Infect Dis*. 2006; 12:15–22. [PubMed: 16494711]
- [17]. Okomo-Adhiambo M, Nguyen HT, Abd Elal A, Sleeman K, Fry AM, Gubareva LV. Drug susceptibility surveillance of influenza viruses circulating in the United States in 2011-2012: application of the WHO antiviral working group criteria. *Influenza and other respiratory viruses*. 2014; 8:258–265. [PubMed: 24299049]
- [18]. Marjuki H, Mishin VP, Chesnokov AP, Jones J, De La Cruz JA, Sleeman K, Tamura D, Nguyen HT, Wu HS, Chang FY, Liu MT, Fry AM, Cox NJ, Villanueva JM, Davis CT, Gubareva LV. Characterization of Drug-Resistant Influenza A(H7N9) Variants Isolated From an Oseltamivir-Treated Patient in Taiwan. *J Infect Dis*. 2014
- [19]. McKimm-Breschkin JL. Influenza neuraminidase inhibitors: antiviral action and mechanisms of resistance. *Influenza and other respiratory viruses*. 2013; 7 Suppl 1:25–36. [PubMed: 23279894]
- [20]. Fiore AE, Fry A, Shay D, Gubareva L, Bresee JS, Uyeki TM, Centers for Disease, C., and Prevention. Antiviral agents for the treatment and chemoprophylaxis of influenza --- recommendations of the Advisory Committee on Immunization Practices (ACIP). *MMWR Recomm Rep*. 2011; 60:1–24. [PubMed: 21248682]
- [21]. Jefferson T, Jones MA, Doshi P, Del Mar CB, Heneghan CJ, Hama R, Thompson MJ. Neuraminidase inhibitors for preventing and treating influenza in healthy adults and children. *Cochrane Database Syst Rev*. 2012; 1:CD008965. [PubMed: 22258996]
- [22]. Torjesen I. Cochrane review questions effectiveness of neuraminidase inhibitors. *BMJ*. 2014; 348:g2675. [PubMed: 24721619]
- [23]. Jefferson T, Doshi P. Multisystem failure: the story of anti-influenza drugs. *BMJ*. 2014; 348:g2263. [PubMed: 24721793]
- [24]. Doshi P, Jefferson T. Clinical trials: Tamiflu reviewers respond to critics. *Nature*. 2014; 509:288. [PubMed: 24828182]
- [25]. Johnson D. Croup. *Clin Evid (Online)* 2009. 2009
- [26]. Bjornson CL, Johnson DW. Croup. *Lancet*. 2008; 371:329–339. [PubMed: 18295000]
- [27]. Salerno D, Hasham MG, Marshall R, Garriga J, Tsygankov AY, Grana X. Direct inhibition of CDK9 blocks HIV-1 replication without preventing T-cell activation in primary human peripheral blood lymphocytes. *Gene*. 2007; 405:65–78. [PubMed: 17949927]

- [28]. Schang LM. First demonstration of the effectiveness of inhibitors of cellular protein kinases in antiviral therapy. *Expert Rev Anti Infect Ther.* 2006; 4:953–956. [PubMed: 17181411]
- [29]. Prussia A, Thepchatri P, Snyder JP, Plemper RK. Systematic Approaches towards the Development of Host-Directed Antiviral Therapeutics. *Int J Mol Sci.* 2011; 12:4027–4052. [PubMed: 21747723]
- [30]. Krumm SA, Ndungu JM, Yoon JJ, Dochow M, Sun A, Natchus M, Snyder JP, Plemper RK. Potent host-directed small-molecule inhibitors of myxovirus RNA-dependent RNA-polymerases. *PLoS ONE.* 2011; 6:e20069. [PubMed: 21603574]
- [31]. Schwegmann A, Brombacher F. Host-directed drug targeting of factors hijacked by pathogens. *Sci Signal.* 2008:1–re8. [PubMed: 18364512]
- [32]. Yan D, Krumm SA, Sun A, Steinhauer DA, Luo M, Moore ML, Plemper RK. Dual myxovirus screen identifies a small-molecule agonist of the host antiviral response. *J Virol.* 2013; 87:11076–11087. [PubMed: 23926334]
- [33]. Buchholz UJ, Finke S, Conzelmann KK. Generation of bovine respiratory syncytial virus (BRSV) from cDNA: BRSV NS2 is not essential for virus replication in tissue culture, and the human RSV leader region acts as a functional BRSV genome promoter. *J Virol.* 1999; 73:251–259. [PubMed: 9847328]
- [34]. Hoffmann E, Neumann G, Kawaoka Y, Hobom G, Webster RG. A DNA transfection system for generation of influenza A virus from eight plasmids. *Proc Natl Acad Sci U S A.* 2000; 97:6108–6113. [PubMed: 10801978]
- [35]. Heaton NS, Leyva-Grado VH, Tan GS, Eggink D, Hai R, Palese P. In vivo bioluminescent imaging of influenza a virus infection and characterization of novel cross-protective monoclonal antibodies. *J Virol.* 2013; 87:8272–8281. [PubMed: 23698304]
- [36]. Manicassamy B, Manicassamy S, Belicha-Villanueva A, Pisanelli G, Pulendran B, Garcia-Sastre A. Analysis of in vivo dynamics of influenza virus infection in mice using a GFP reporter virus. *Proc Natl Acad Sci U S A.* 2010; 107:11531–11536. [PubMed: 20534532]
- [37]. Donnelly ML, Hughes LE, Luke G, Mendoza H, ten Dam E, Gani D, Ryan MD. The 'cleavage' activities of foot-and-mouth disease virus 2A site-directed mutants and naturally occurring '2A-like' sequences. *The Journal of general virology.* 2001; 82:1027–1041. [PubMed: 11297677]
- [38]. Hotard AL, Shaikh FY, Lee S, Yan D, Teng MN, Plemper RK, Crowe JE Jr, Moore ML. A stabilized respiratory syncytial virus reverse genetics system amenable to recombination-mediated mutagenesis. *Virology.* 2012; 434:129–136. [PubMed: 23062737]
- [39]. Chung HK, Jacobs CL, Huo Y, Yang J, Krumm SA, Plemper RK, Tsien RY, Lin MZ. Tunable and reversible drug control of protein production via a self-excising degron. *Nat Chem Biol.* 2015 [Epub ahead of print].
- [40]. Jacob RT, Larsen MJ, Larsen SD, Kirchhoff PD, Sherman DH, Neubig RR. MScreen: an integrated compound management and high-throughput screening data storage and analysis system. *J Biomol Screen.* 2012; 17:1080–1087. [PubMed: 22706349]
- [41]. Zhang JH, Chung TD, Oldenburg KR. A Simple Statistical Parameter for Use in Evaluation and Validation of High Throughput Screening Assays. *J Biomol Screen.* 1999; 4:67–73. [PubMed: 10838414]
- [42]. Boutros M, Bras LP, Huber W. Analysis of cell-based RNAi screens. *Genome Biol.* 2006; 7:R66. [PubMed: 16869968]
- [43]. Tran V, Moser LA, Poole DS, Mehle A. Highly sensitive real-time in vivo imaging of an influenza reporter virus reveals dynamics of replication and spread. *J Virol.* 2013; 87:13321–13329. [PubMed: 24089552]
- [44]. Lazarowitz SG, Goldberg AR, Choppin PW. Proteolytic cleavage by plasmin of the HA polypeptide of influenza virus: host cell activation of serum plasminogen. *Virology.* 1973; 56:172–180. [PubMed: 4795670]
- [45]. Yan D, Lee S, Thakkar VD, Luo M, Moore ML, Plemper RK. Cross-resistance mechanism of respiratory syncytial virus against structurally diverse entry inhibitors. *Proc Natl Acad Sci U S A.* 2014; 111:E3441–3449. [PubMed: 25092342]
- [46]. Scola PM, Sun LQ, Wang AX, Chen J, Sin N, Venables BL, Sit SY, Chen Y, Cocuzza A, Bilder DM, D'Andrea SV, Zheng B, Hewawasam P, Tu Y, Friborg J, Falk P, Hernandez D, Levine S,

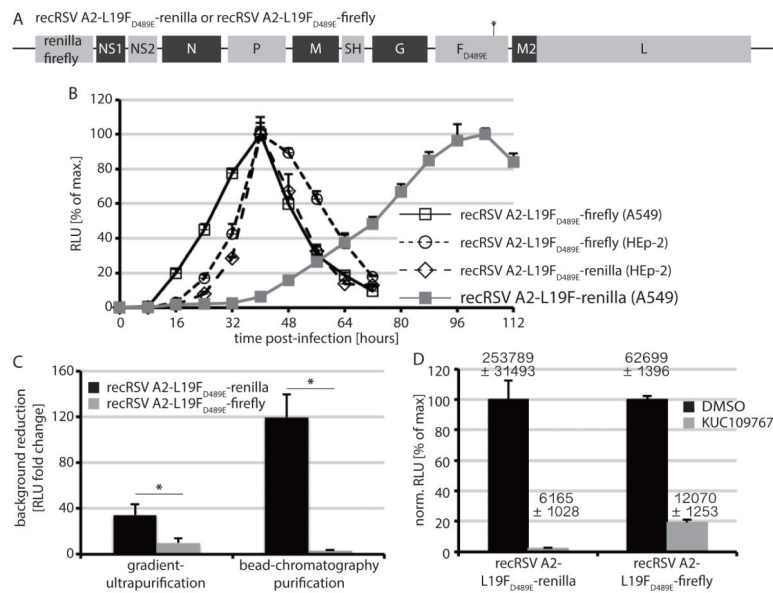
- Chen C, Yu F, Sheaffer AK, Zhai G, Barry D, Knipe JO, Han YH, Schartman R, Donoso M, Mosure K, Sinz MW, Zvyaga T, Good AC, Rajamani R, Kish K, Tredup J, Klei HE, Gao Q, Mueller L, Colonno RJ, Grasela DM, Adams SP, Loy J, Levesque PC, Sun H, Shi H, Sun L, Warner W, Li D, Zhu J, Meanwell NA, McPhee F. The discovery of asunaprevir (BMS-650032), an orally efficacious NS3 protease inhibitor for the treatment of hepatitis C virus infection. *J Med Chem.* 2014; 57:1730–1752. [PubMed: 24564672]
- [47]. Zhang JH, Chung TDY, Oldenburg KR. A simple statistical parameter for used in evaluation and validation of high throughput screening assays. *J Biomol Screen.* 1999; 4:67–73. [PubMed: 10838414]
- [48]. Cianci C, Yu KL, Combrink K, Sin N, Pearce B, Wang A, Civiello R, Voss S, Luo G, Kadow K, Genovesi EV, Venables B, Gulgeze H, Trehan A, James J, Lamb L, Medina I, Roach J, Yang Z, Zadjura L, Colonno R, Clark J, Meanwell N, Krystal M. Orally active fusion inhibitor of respiratory syncytial virus. *Antimicrob Agents Chemother.* 2004; 48:413–422. [PubMed: 14742189]
- [49]. Denisova OV, Kakkola L, Feng L, Stenman J, Nagaraj A, Lampe J, Yadav B, Aittokallio T, Kaukinen P, Ahola T, Kuivanen S, Vapalahti O, Kantele A, Tynell J, Julkunen I, Kallio-Kokko H, Paavilainen H, Hukkanen V, Elliott RM, De Brabander JK, Saelens X, Kainov DE. Obatoclox, saliphenylhalamide, and gemcitabine inhibit influenza a virus infection. *J Biol Chem.* 2012; 287:35324–35332. [PubMed: 22910914]
- [50]. Clouser CL, Holtz CM, Mullett M, Crankshaw DL, Briggs JE, O'Sullivan MG, Patterson SE, Mansky LM. Activity of a novel combined antiretroviral therapy of gemcitabine and decitabine in a mouse model for HIV-1. *Antimicrob Agents Chemother.* 2012; 56:1942–1948. [PubMed: 22271861]
- [51]. Arteaga CL, Brown TD, Kuhn JG, Shen HS, O'Rourke TJ, Beougher K, Brentzel HJ, Von Hoff DD, Weiss GR. Phase I clinical and pharmacokinetic trial of Brequinar sodium (DuP 785; NSC 368390). *Cancer Res.* 1989; 49:4648–4653. [PubMed: 2743343]
- [52]. Nichol CA, Welch AD. On the mechanism of action of aminopterin. *Proc Soc Exp Biol Med.* 1950; 74:403–411. [PubMed: 15440837]
- [53]. Beylveeld G, White KM, Ayllon J, Shaw ML. New-generation screening assays for the detection of anti-influenza compounds targeting viral and host functions. *Antiviral Res.* 2013; 100:120–132. [PubMed: 23933115]
- [54]. DeVincenzo JP, Whitley RJ, Mackman RL, Scaglioni-Weinlich C, Harrison L, Farrell E, McBride S, Lambkin-Williams R, Jordan R, Xin Y, Ramanathan S, O'Riordan T, Lewis SA, Li X, Toback SL, Lin SL, Chien JW. Oral GS-5806 activity in a respiratory syncytial virus challenge study. *The New England journal of medicine.* 2014; 371:711–722. [PubMed: 25140957]
- [55]. Samuel D, Xing W, Niedziela-Majka A, Wong J, Brendza K, Jordan R, Perron M, Sperandio D, Liu X, Sakowicz R, Mackman R. V-1814. GS-5806 Inhibits Pre- to Post-fusion Conformational Changes of the RSV Fusion Protein. *Interscience Conference of Antimicrobial Agents and Chemotherapy.* 2014
- [56]. Weisshaar M, Cox R, Plemper RK. Blocking Respiratory Syncytial Virus Entry: A Story with Twists. *DNA Cell Biol.* 2015
- [57]. Hallak LK, Spillmann D, Collins PL, Peeples ME. Glycosaminoglycan sulfation requirements for respiratory syncytial virus infection. *J Virol.* 2000; 74:10508–10513. [PubMed: 11044095]
- [58]. Shanley JD, Debs RJ. The folate antagonist, methotrexate, is a potent inhibitor of murine and human cytomegalovirus in vitro. *Antiviral Research.* 1989; 11:99–106. [PubMed: 2543289]
- [59]. Hoffmann HH, Kunz A, Simon VA, Palese P, Shaw ML. Broad-spectrum antiviral that interferes with de novo pyrimidine biosynthesis. *Proc Natl Acad Sci U S A.* 2011; 108:5777–5782. [PubMed: 21436031]
- [60]. Guilbault C, De Sanctis JB, Wojewodka G, Saeed Z, Lachance C, Skinner TA, Vilela RM, Kubow S, Lands LC, Hajduch M, Matouk E, Radzioch D. Fenretinide corrects newly found ceramide deficiency in cystic fibrosis. *American journal of respiratory cell and molecular biology.* 2008; 38:47–56. [PubMed: 17656682]
- [61]. Finnegan CM, Blumenthal R. Fenretinide inhibits HIV infection by promoting viral endocytosis. *Antiviral Res.* 2006; 69:116–123. [PubMed: 16375981]

- [62]. Fraser JE, Rawlinson SM, Wang C, Jans DA, Wagstaff KM. Investigating dengue virus nonstructural protein 5 (NS5) nuclear import. *Methods Mol Biol.* 2014; 1138:301–328. [PubMed: 24696345]
- [63]. Beaudry H, Gendron L, Moron JA. Implication of delta opioid receptor subtype 2 but not delta opioid receptor subtype 1 in the development of morphine analgesic tolerance in a rat model of chronic inflammatory pain. *Eur J Neurosci.* 2015; 41:901–907. [PubMed: 25639561]
- [64]. Charbaji N, Schafer-Korting M, Kuchler S. Morphine stimulates cell migration of oral epithelial cells by delta-opioid receptor activation. *PLoS One.* 2012; 7:e42616. [PubMed: 22900034]
- [65]. Salimi V, Hennis MP, Mokhtari-Azad T, Shokri F, Janssen R, Hodemaekers HM, Rygiel TP, Coenjaerts FE, Meyaard L, Bont L. Opioid receptors control viral replication in the airways. *Crit Care Med.* 2013; 41:205–214. [PubMed: 23222260]
- [66]. Tsai CY, Ray AS, Tumas DB, Keating MJ, Reiser H, Plunkett W. Targeting DNA repair in chronic lymphocytic leukemia cells with a novel acyclic nucleotide analogue, GS-9219. *Clin Cancer Res.* 2009; 15:3760–3769. [PubMed: 19435836]
- [67]. Wolfgang GH, Shibata R, Wang J, Ray AS, Wu S, Doerrfler E, Reiser H, Lee WA, Birkus G, Christensen ND, Andrei G, Snoeck R. GS-9191 is a novel topical prodrug of the nucleotide analog 9-(2-phosphonylmethoxyethyl)guanine with antiproliferative activity and possible utility in the treatment of human papillomavirus lesions. *Antimicrob Agents Chemother.* 2009; 53:2777–2784. [PubMed: 19398642]
- [68]. Vail DM, Thamm DH, Reiser H, Ray AS, Wolfgang GH, Watkins WJ, Babusis D, Henne IN, Hawkins MJ, Kurzman ID, Jeraj R, Vanderhoek M, Plaza S, Anderson C, Wessel MA, Robat C, Lawrence J, Tumas DB. Assessment of GS-9219 in a pet dog model of non-Hodgkin's lymphoma. *Clin Cancer Res.* 2009; 15:3503–3510. [PubMed: 19417014]
- [69]. Zhang J, Stevens MF, Bradshaw TD. Temozolomide: mechanisms of action, repair and resistance. *Curr Mol Pharmacol.* 2012; 5:102–114. [PubMed: 22122467]
- [70]. Gribaudo G, Riera L, Lembo D, De Andrea M, Johnson LF, Landolfo S. The anticytomegaloviral activity of raltitrexed is abrogated in quiescent mouse fibroblasts that overexpress thymidylate synthase. *Virus Res.* 2001; 73:57–65. [PubMed: 11163644]
- [71]. Guerrero CA, Murillo A, Acosta O. Inhibition of rotavirus infection in cultured cells by N-acetylcysteine, PPARgamma agonists and NSAIDs. *Antiviral Research.* 2012; 96:1–12. [PubMed: 22842004]
- [72]. Morlet N, Stayt J, Vaegan, Salonikas C, Naidoo D, Crouch R, Graham G, Coroneo M. Etoposide as a virocidal anticytomegalovirus therapy: intravitreal toxicology and pharmacology in rabbits. *Aust N Z J Ophthalmol.* 1999; 27:342–349. [PubMed: 10571395]
- [73]. Mohammadgholi A, Rabbani-Chadegani A, Fallah S. Mechanism of the interaction of plant alkaloid vincristine with DNA and chromatin: spectroscopic study. *DNA Cell Biol.* 2013; 32:228–235. [PubMed: 23590199]
- [74]. Loh PC, Soergel M. Growth characteristics of reovirus type 2: actinomycin D and the synthesis of viral RNA. *Proceedings of the National Academy of Sciences of the United States of America.* 1965; 54:857–863. [PubMed: 5217464]
- [75]. Wan Z, Chen X. Triptolide inhibits human immunodeficiency virus type 1 replication by promoting proteasomal degradation of Tat protein. *Retrovirology.* 2014; 11:88. [PubMed: 25323821]
- [76]. Cova LT,C, Narayan R, Borowski P, Kulikowski T, Zagorski-Ostojka W, Register EP. Epirubicine hydrochloride for treating hepatitis C virus. 2006
- [77]. Cao J, Forrest JC, Zhang X. A screen of the NIH Clinical Collection small molecule library identifies potential anti-coronavirus drugs. *Antiviral Research.* 2015; 114:1–10. [PubMed: 25451075]
- [78]. Patel DA, Patel AC, Nolan WC, Zhang Y, Holtzman MJ. High throughput screening for small molecule enhancers of the interferon signaling pathway to drive next-generation antiviral drug discovery. *PLoS One.* 2012; 7:e36594. [PubMed: 22574190]
- [79]. Fischer MA, Smith JL, Shum D, Stein DA, Parkins C, Bhinder B, Radu C, Hirsch AJ, Djaballah H, Nelson JA, Fruh K. Flaviviruses are sensitive to inhibition of thymidine synthesis pathways. *Journal of virology.* 2013; 87:9411–9419. [PubMed: 23824813]

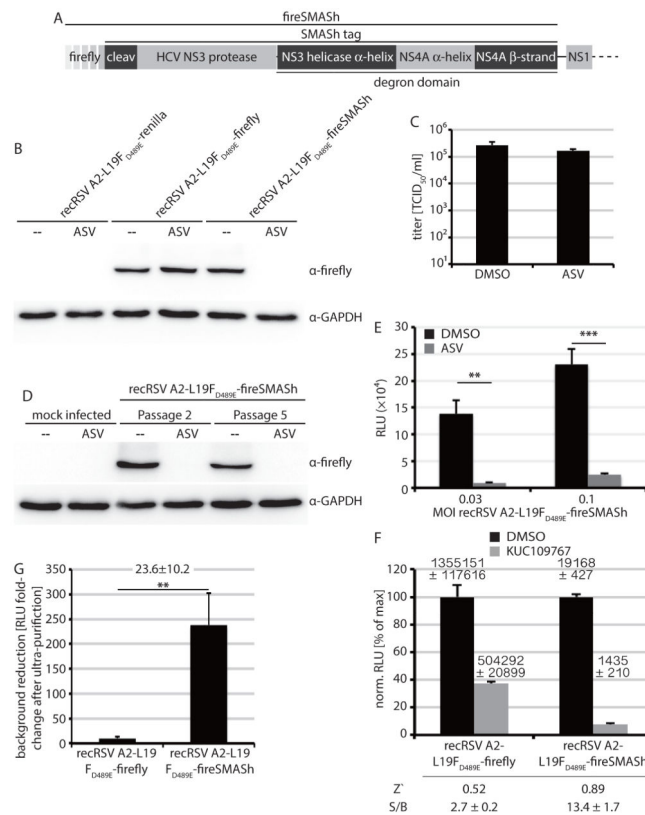
- [80]. Sidwell RW, Arnett G, Schabel FM Jr. In vitro effect of a variety of biologically active compounds on human cytomegalovirus. *Chemotherapy*. 1972; 17:259–282. [PubMed: 4339265]
- [81]. Yeo KL, Chen YL, Xu HY, Dong H, Wang QY, Yokokawa F, Shi PY. Synergistic suppression of dengue virus replication using a combination of nucleoside analogs and nucleoside synthesis inhibitors. *Antimicrobial Agents and Chemotherapy*. 2015; 59:2086–2093. [PubMed: 25624323]
- [82]. Lucas-Hourani M, Dauzonne D, Jorda P, Cousin G, Lupan A, Helynck O, Caignard G, Janvier G, Andre-Leroux G, Khiar S, Escriou N, Despres P, Jacob Y, Munier-Lehmann H, Tangy F, Vidalain PO. Inhibition of pyrimidine biosynthesis pathway suppresses viral growth through innate immunity. *PLoS pathogens*. 2013; 9:e1003678. [PubMed: 24098125]
- [83]. Demicheli V, Jefferson T, Rivetti D, Deeks J. Prevention and early treatment of influenza in healthy adults. *Vaccine*. 2000; 18:957–1030. [PubMed: 10590322]
- [84]. Smee DF, Bray M, Huggins JW. Antiviral activity and mode of action studies of ribavirin and mycophenolic acid against orthopoxviruses in vitro. *Antiviral chemistry & chemotherapy*. 2001; 12:327–335. [PubMed: 12018677]
- [85]. Fox T, Coll JT, Xie X, Ford PJ, Germann UA, Porter MD, Pazhanisamy S, Fleming MA, Galullo V, Su MS, Wilson KP. A single amino acid substitution makes ERK2 susceptible to pyridinyl imidazole inhibitors of p38 MAP kinase. *Protein Sci*. 1998; 7:2249–2255. [PubMed: 9827991]
- [86]. Matharu DS, Flaherty DP, Simpson DS, Schroeder CE, Chung D, Yan D, Noah JW, Jonsson CB, White EL, Aube J, Plemper RK, Severson WE, Golden JE. Optimization of potent and selective quinazolinones: inhibitors of respiratory syncytial virus that block RNA-dependent RNA-polymerase complex activity. *J Med Chem*. 2014; 57:10314–10328. [PubMed: 25399509]
- [87]. Yan D, Lee S, Thakkar VD, Luo M, Moore ML, Plemper RK. Cross-resistance mechanism of respiratory syncytial virus against structurally diverse entry inhibitors. *Proceedings of the National Academy of Sciences of the United States of America*. 2014
- [88]. Krumm SA, Yan D, Hovingh ES, Evers TJ, Enkirch T, Reddy GP, Sun A, Saindane MT, Arrendale RF, Painter G, Liotta DC, Natchus MG, von Messling V, Plemper RK. An orally available, small-molecule polymerase inhibitor shows efficacy against a lethal morbillivirus infection in a large animal model. *Science translational medicine*. 2014; 6:232ra252.
- [89]. Yoon JJ, Krumm SA, Ndungu JM, Hoffman V, Bankamp B, Rota PA, Sun A, Snyder JP, Plemper RK. Target analysis of the experimental measles therapeutic AS-136A. *Antimicrob Agents Chemother*. 2009; 53:3860–3870. [PubMed: 19528268]

**Figure 1.**

Generation of a recIAV WSN-NanoLuc reporter strain. A) Schematic of the WSN PB2-NanoLuc or PB2-Gaussia genome segment (PS*: downstream packaging signal that was inactivated through silent mutagenesis; 2A PTV-derived cleavage site; NanoLuc or Gaussia: luciferase ORF; KDEL: ER retention signal; and PS: engineered packaging signal. Grey shading specifies the reading frame of the engineered segment. Individual segments are not drawn to scale. B) Reporter expression profile of IAV WSN-Gaussia on A549 cells ($N = 3$; means \pm SD are shown). Instrument gain 250; RLU (relative luciferase unit) C) Signal window of the recIAV WSN-Gaussia and analogous recIAV WSN-NanoLuc reporter strains. A549 cells were exposed at infection to the potent inhibitor 5-iodotubercidin⁸⁵ at 10 μ M or the vehicle (DMSO) volume equivalent. RLUs were determined 48 hours post-infection. Values were normalized for vehicle controls ($N = 3$; means \pm SD are shown); numbers above the columns show raw data means \pm SD. Z' and S/B values are specified below the graph. D) Reporter expression profiles of recIAV WSN-NanoLuc as in (B) after infection of A549 cells at two different MOIs ($N = 3$; means \pm SD are shown). Instrument gain 135 for recIAV WSN-NanoLuc. The IAV WSN-Gaussia profile was added for comparison. E) recIAV WSN-NanoLuc and WSN-Gaussia are genetically stable over several passages. Progeny viral titers were determined by plaque assay (left panel) and TCID₅₀ titration using luciferase activity as the read-out (right panel) after each passage ($N = 3$; means \pm SD are shown).

**Figure 2.**

Development of second-generation recRSV reporter strains. A) Schematic of the recRSV-L19F_{D489E}-firefly and renilla luciferase genomes. B) Reporter expression profile after infection with recRSV-L19F-*renilla* or newly generated recRSV-L19F_{D489E}-firefly or recRSV-L19F_{D489E}-*renilla* (MOI 0.3 each; instrument gain 200). Values represent cell-associated luciferase activities and were normalized to the highest signal of each series ($N = 3$; means \pm SD are shown). Purification of recRSV-L19F_{D489E}-firefly and recRSV-L19F_{D489E}-*renilla* progeny virions through different techniques. RLU in virus stocks before and after purification were determined and background clearance ($RLU_{\text{before}}/RLU_{\text{after}}$) calculated ($N = 3$; means \pm SD are shown; 2-tailed t-test, *: $p < 0.05$). D) Signal window of the recRSV reporter strains. A549 cells were exposed at infection to 10 μ M KUC109767, an inhibitor of RSV RdRp activity⁸⁶, or the vehicle (DMSO) volume equivalent. RLU were determined 44 hours post-infection and values normalized for vehicle controls ($N = 3$; means \pm SD are shown); numbers above the columns show raw data means \pm SD.

**Figure 3.**

recRSV-L19F_{D489E}-fireSMASH allows induced reporter degradation. A) Schematic of the fireSMASH cassette inserted into the recRSV-L19F_{D489E} genome (cleav: HCV NS3 cleavage site). B) Immunodetection of firefly luciferase after infection of cells with the specified recRSV-L19F_{D489E} strain in the presence or absence of the NS3 inhibitor asunaprevir (ASV) and SDS-PAGE of cell lysates. Cellular GAPDH levels were determined as loading controls. C) Peak recRSV-L19F_{D489E}-fireSMASH progeny titers after incubation in the presence of 3 μM ASV or vehicle (DMSO). (*N* = 3; means ± SD are shown). D) Immunodetection of firefly luciferase after serial passaging of recRSV-L19F_{D489E}-fireSMASH and reinfection of cells in the presence or absence of 3 μM ASV. Passage 2 (P2) and passage 5 (P5) are shown, GAPDH levels were determined as loading controls. E) Firefly activity after growth of recRSV-L19F_{D489E}-fireSMASH in the presence or absence of 3 μM ASV. Cells were infected at the specified MOIs and harvested 44 hours post-infection (*N* = 3; means ± SD are shown; 2-tailed t-test, **: *p* < 0.01; ***: *p* < 0.001). F) Signal window of the recRSV-L19F_{D489E}-fireSMASH reporter strain was calculated as described in figure 2D (*N* = 3; means ± SD are shown); numbers above the columns show raw data means ± SD. *Z'* and *S/B* values are specified below the graph. G) Fold-change of contaminating firefly luciferase after gradient purification of recRSV-L19F_{D489E}-firefly and recRSV-L19F_{D489E}-fireSMASH preparation to unpurified recRSV-L19F_{D489E}-firefly (*N* = 3; means ± SD are shown; 2-tailed t-test; **: *p* < 0.01).

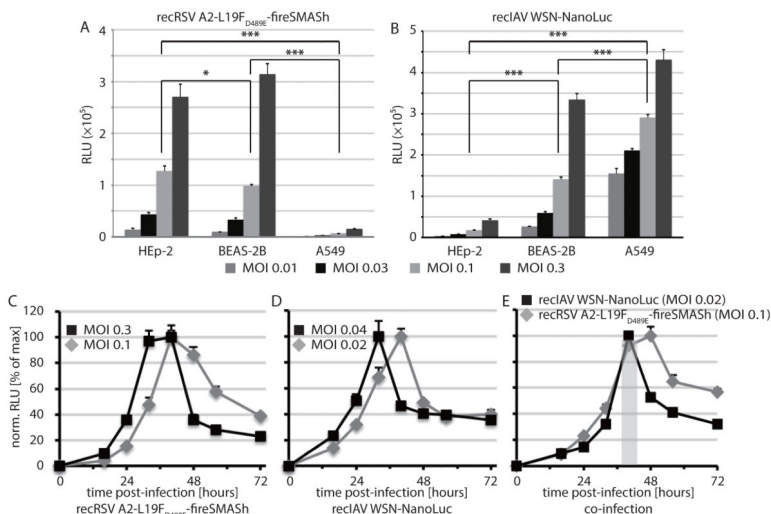
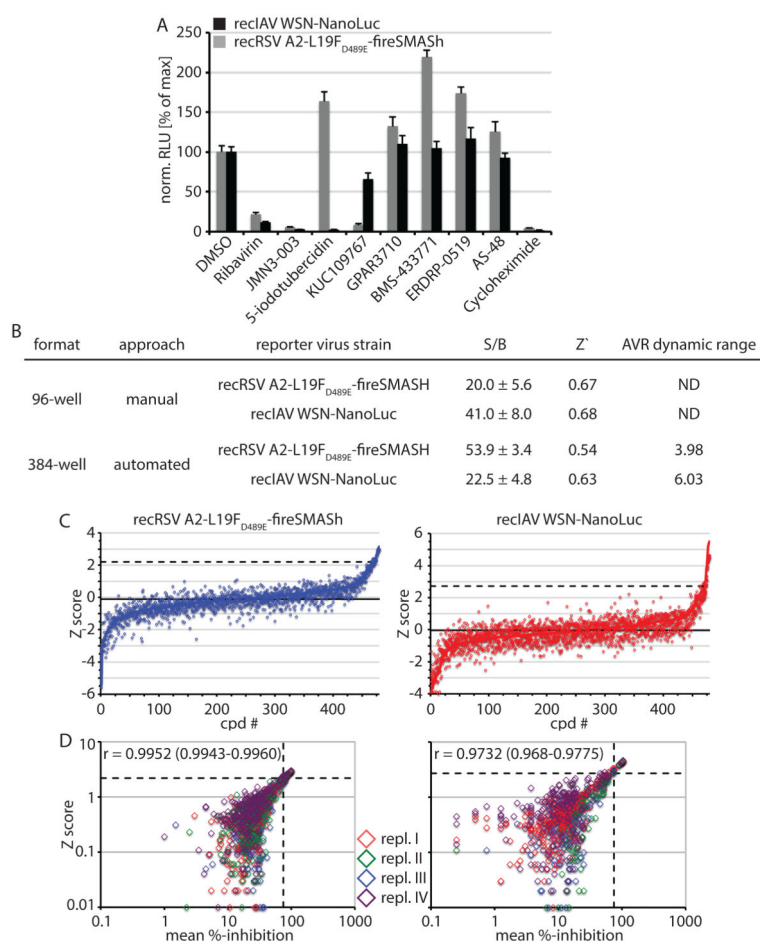


Figure 4. Infection conditions for synchronized RSV and IAV reporter expression. A and B) Luciferase activities in three different human respiratory host cell lines 44 hours post-infection at the specified MOIs with recRSV-L19F_{D489E}-fireSMASH (A) or recIAV WSN-NanoLuc (B; $N = 4$; means \pm SD are shown). Two-way ANOVA with Tukey’s multiple comparison post-tests were carried out to assess statistical significance of sample divergence. Results are shown for MOI 0.1 (A) and 0.04 (B); *: $p < 0.05$; ***: $p < 0.01$. C- E) Reporter activity profiles after infection of BEAS-2B cells singly with recRSV-L19F_{D489E}-fireSMASH (C) or recIAV WSN-NanoLuc (D), or after co-infection with both strains at an MOI of 0.1 (RSV) and 0.02 (IAV), respectively (E). Values represent cell-associated luciferase activities and were normalized to the highest signal of each series ($N = 3$; means \pm SD are shown); grey shaded area in (D) marks the time window post-infection when signal intensities of both luciferase reporters are $\geq 80\%$ of max.

**Figure 5.**

Assay miniaturization and validation. A) Co-infection of BEAS-2B cells with recRSV-L19F_{D489E}-fireSMASH and recIAV WSN-NanoLuc as specified in figure 4E in a 96-well plate format. Known RSV-specific (KUC109767 (10 μ M)⁸⁶, GPAR3710 (10 μ M)⁸⁷, and BMS-433771 (10 μ M)⁴⁸) IAV-specific (5-iodotubercidin (10 μ M)⁸⁵), and MeV-specific inhibitors (ERDRP-0519 (10 μ M)⁸⁸, AS-48 (40 μ M)⁸⁹), broad-spectrum antivirals (ribavirin (40 μ M) and JMN3-003 (10 μ M)³⁰), and cytotoxic cycloheximide (100 μ g/ml) were used for assay validation ($N = 5$; means \pm SD are shown). B) Co-infection assay parameters obtained in 96-well (manual; one plate each; $N = 5$; means \pm SD are shown) and 384-well (automated; four plates each; $N = 128$; means \pm SD are shown) format. The broad-spectrum myxovirus inhibitor JMN3-003³⁰ was used as a reference compound. AVR dynamic range: mean dynamic range across all replicate plates; ND: not determined. C) Z-score profiles of automated dual-pathogen pilot screens of the NCC collection in 384-well plate format in four replicates. Symbols mark Z-scores of individual replicate screens, solid black lines represent the assay Z-score mean, and dashed black lines show the hit cut-off (assay mean + 2.5 \times (assay Z-score SD)). Final screening concentration was 5 μ M. D) Individual Z-scores of the replicate (repl. I-IV) screens shown in (C) are plotted as a function of the mean %-inhibition for each compound. Dashed horizontal and vertical black lines show hit cut-offs based on Z-score (assay mean + 2.5 \times (assay Z-score SD)) and

biological effect (mean inhibition >75%), respectively. Numbers represent Pearson correlation coefficients (r) and 95% confidence intervals.

Author Manuscript

Author Manuscript

Author Manuscript

Author Manuscript

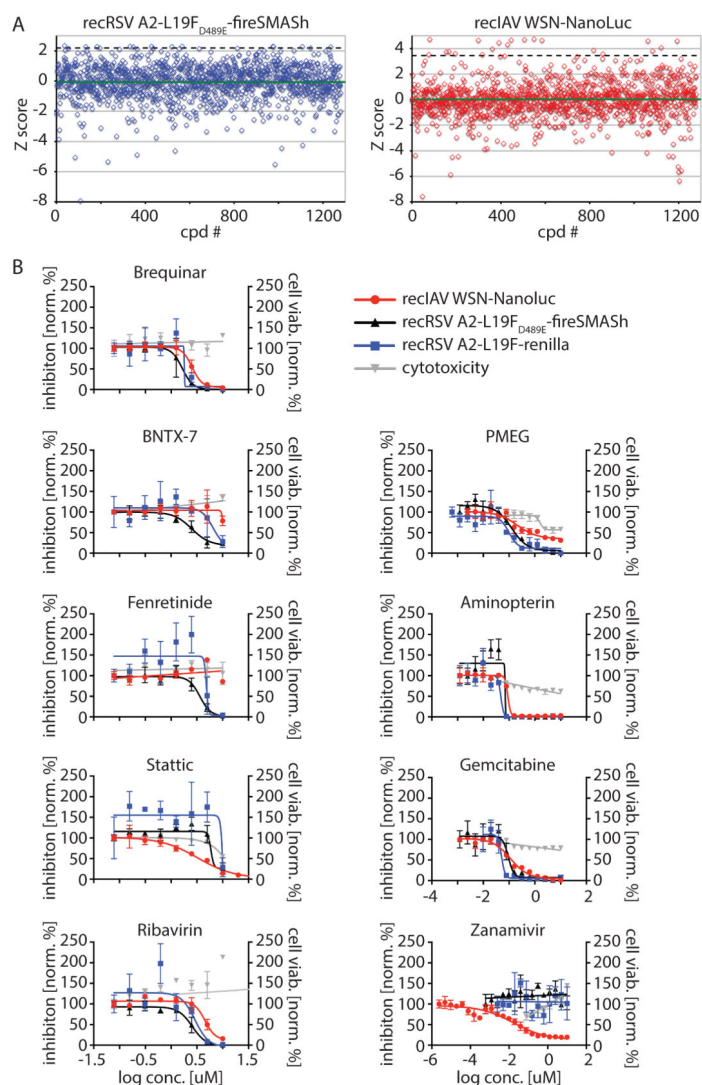


Figure 6. Test screen of a 1280-compound LOPAC library of known bioactives (overall $Z' = 0.31$). A) Z-score profiles of the automated proof-of-concept screen of the LOPAC library in 384-well format. Solid green lines show Z-score means, dashed black lines hit cut-offs (assay mean + $2.0 \times$ (assay Z-score SD) for recRSV A2-L19F_{D489E}-fireSMASH, assay mean + $2.5 \times$ (assay Z-score SD) for rec IAV WSN-NanoLuc). Final screening concentration was 5 μM . B) Dose-response assays of hit candidates in a concentration (conc.) range of 10-0.078 or 10-0.0006 μM . Only hits with CC_{50} concentrations $\leq 10 \mu\text{M}$ and confirmed inhibition of at least one primary target virus are shown. Values were normalized (norm.) for vehicle (DMSO)-treated infections and represent mean % inhibition or % cell viability (viab.) of three replicates \pm SD. Regressions curves for antiviral (black) or cytotoxic (grey) activities are based on four-parameter modeling where applicable.

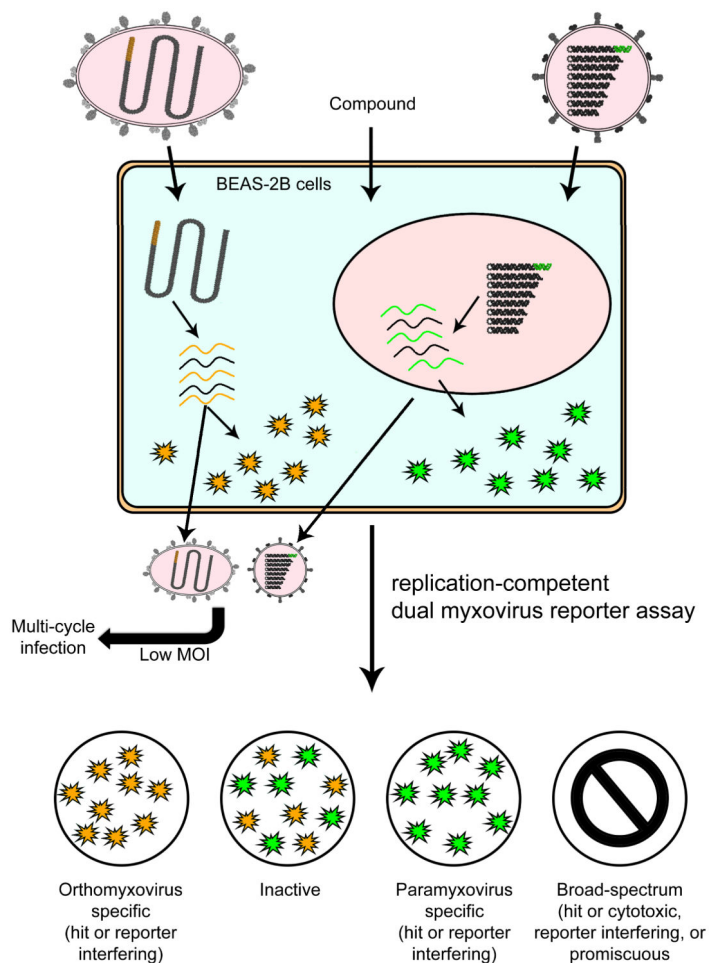


Figure 7. Overview of the replication-competent IAV and RSV reporter strain-based next-generation dual pathogen HTS protocol for the simultaneous identification of IAV-specific, RSV-specific, and broad spectrum inhibitors. The assay is validated for human respiratory BEAS-2B cells, but adaptable to all cell lines that are permissive for either virus strain. Infection at high MOI will predominantly identify inhibitors of viral entry and polymerase, while low MOI multi-cycle infections allow interrogation of all stages of the viral live cycle. Counterscreens are required to distinguish between hit candidates or reporter interfering compounds (specific antiviral activity), and hit candidates, reporter interfering compounds, cytotoxic compounds, or promiscuous pan-assay interfering (PAIN) compounds (broad spectrum activity).

Table 1

Primary screening hit candidates of the NCC collection, based on automated screening of the library in four replicates in 384-well format. Results are grouped by RSV-specific hit candidates, IAV-specific hit candidates, and inhibitors of both target viruses.

Name	% Inhibition (anti-RSV) ¹	% Inhibition (anti-IAV) ²	Bioactivity/ Biological target ³	Known Antiviral Targets ⁴
RSV predominant				
Temozolomide	96 ± 1.3	55 ± 3.2	DNA replication ⁶⁹	None
Raltitrexed	91 ± 1.0	60 ± 6.5	Thymidylate synthase ⁷⁰	Cytomegaloviruses ⁷⁰
Rosiglitazone	85 ± 5.8	35 ± 5	Adenomatosis polyposis coli 2 Eukaryotic translation initiation factor 5A-1 Peroxisome proliferator-activated receptor-gamma ⁷¹	Rotaviruses ⁷¹
Etoposide	80 ± 6.6	56 ± 5.6	DNA topoisomerase II ⁷²	Cytomegaloviruses ⁷²
Vincristine	79 ± 6.9	50 ± 2.9	Microtubule assembly ⁷³	None
IAV predominant				
Actinomycin D	52 ± 9.6	104 ± 1.5	RNA synthesis ⁷⁴	Reovirus type 2 ⁷⁴
Triptolide	1.5 ± 21	103 ± 1.2	XPB (a subunit of TFIIH) ⁷⁵	HIV-1 ⁷⁵
Epirubicin	62 ± 6.3	75 ± 3.1	DNA intercalator (104)	Heptatitis C ⁷⁶
Inhibition of both reporter strains				
Methotrexate	99 ± 0.5	100 ± 0.6	Dihydrofolate reductase, Deoxycytidine kinase ⁵⁸	Murine and human cytomegalovirus ⁵⁸
Homoharringtonine	98 ± 0.5	90 ± 2.6	60S ribosome inhibitor ⁷⁷	Recombinant murine coronavirus ⁷⁷
Idarubicin	95 ± 1.3	97 ± 1	DNA topoisomerase II ⁷⁸	Encephalomyocarditis virus (EMCV) ⁷⁸

¹ based on four independent replicate screens; mean % inhibition ± SD are shown.

² based on four independent replicate screens; mean % inhibition ± SD are shown.

³ previously proposed activity, target, and antiviral spectrum, if known

⁴ previously proposed activity, target, and antiviral spectrum, if known

Table 2

Dose-response counterscreening of hit candidates identified through automated screening of the LOPAC1280 library in single replicate in 384-well format.

Name	EC ₅₀ ^a IAV WSN- nanoLuc [μM]	EC ₅₀ ^a RSV A2-L19F- renilla [μM]	EC ₅₀ ^a RSV A2- L19F _{D489E} - fireSMASH [μM]	CC ₅₀ ^a (PrestoBlue cell viability) [μM]	Proposed target/ bioactivity	SI [CC ₅₀ /EC ₅₀] Comment
Aminopterin	0.09 (0.07- 0.11)	0.05 (0.03- 0.07)	0.07	10	dihydrofolate reductase/purine synthesis	SI _{IAV} 111 SI _{RSV} 143 conf. broad spectrum ^{79, 80}
Brequinar	2.6 (2.3-2.9)	1.8	1.6 (1.3-2.1)	>10 ^b	DHODH/pyrimidine synthesis	SI _{IAV} >3.8 SI _{RSV} >6.3 conf. broad spectrum ^{81, 82}
Gemcitabine	0.1 (0.09-0.14)	0.05 (0.04- 0.06)	0.09 (0.07-0.12)	>10	nucleoside analog	SI _{IAV} >100 SI _{RSV} >111 HIV, IAV ^{49, 50}
Zanamivir	0.02 (0.01- 0.04)	Inactive	Inactive	>10 ^b	neuraminidase	SI _{IAV} >500 IAV inhibitor ⁸³
Calcimycin	n.d. ^c	n.d. ^c	n.d. ^c	tox ^d	cation ionophore	tox discarded
Emetine	n.d. ^c	n.d. ^c	n.d. ^c	tox ^d	ribosome	tox discarded
ET-18-OCH3	inactive ^e	inactive ^e	inactive ^e	>10 ^b	PIPLC/PKC	failed conf.
Sunitinib	n.d. ^c	n.d. ^c	n.d. ^c	tox ^d	RTKs	tox discarded
Idarubicin	n.d. ^c	n.d. ^c	n.d. ^c	tox ^d	topoisomerase	tox discarded
Fenretinide	inactive ^e	4.8	3.6 (2.9-4.6)	>10 ^b	activation of stress kinases; induces autophagy	SI _{RSV} >2.8 Dengue ⁶² , HIV ⁶¹
BNTX-7	inactive ^e	6.5 (0.14-307)	2.5 (1.8-3.6)	>10 ^b	DOR1	SI _{RSV} >4
Lometrexol	n.d. ^c	n.d. ^c	n.d. ^c	tox ^d	purine synthesis	tox discarded
PMEG	0.2 (0.1-0.4)	0.1 (0.07-0.15)	0.1 (0.09-0.18)	10	acyclic nucleotide analog	SI _{IAV} 50 SI _{RSV} 100 HPV ⁶⁷
Nitrendipine	inactive ^e	inactive ^e	inactive ^e	>10 ^b	dihydropyridine calcium channel	failed conf.
PD173952	n.d. ^c	n.d. ^c	n.d. ^c	tox ^d	Src kinase	tox discarded
K114	inactive ^e	inactive ^e	inactive ^e	>10 ^b	amyloid-specific dye	failed conf.
Phenanthroline	n.d. ^c	n.d. ^c	n.d. ^c	2.4 ^d	metalloproteases	tox discarded
Auranofin	n.d. ^c	n.d. ^c	n.d. ^c	tox ^d	TLR signaling	tox discarded
Sanguinarine	n.d. ^c	n.d. ^c	n.d. ^c	tox ^d	Na/K ATPase	tox discarded
Stattic	3.3 (2.2-5.1)	15.1	5.9	10	STAT3	SI _{IAV} 3
PD-166285	n.d. ^c	n.d. ^c	n.d. ^c	tox ^d	RTKs	tox discarded

Name	EC ₅₀ ^a IAV WSN- nanoLuc [μ M]	EC ₅₀ ^a RSV A2-L19F- renilla [μ M]	EC ₅₀ ^a RSV A2- L19F _{D489E} - fireSMASH [μ M]	CC ₅₀ ^a (PrestoBlue cell viability) [μ M]	Proposed target/ bioactivity	SI [CC ₅₀ /EC ₅₀] Comment
Ribavirin	4.5 (2.9-5.3)	2.9 (1.6-5.4)	2.6 (2.1-3.2)	>10 ^b	nucleoside analog	SI _{IAV} >2.2 SI _{RSV} >3.9 broad spectrum ⁸⁴
Triamterene	inactive ^e	inactive ^e	inactive ^e	>10 ^b	epithelial Na ⁺ channel	failed conf.
BIX 01294	inactive ^e	inactive ^e	inactive ^e	>10 ^b	histone methyltransferase	failed conf.
Triptolide	0.15 (0.11- 0.21)	0.6	0.4 (0.3-0.5)	0.3 (0.22-0.4)	XPB (a subunit of TFIIH)	tox discarded

^a calculated through four-parameter variable slope regression modeling. Raw values are based on luciferase reporter expression and represent means of three independent replicates calculated EC₅₀ concentrations and 95% confidence intervals are shown

^b highest concentration assessed 10 μ M

^c not determined based on initial cell viability testing

^d less than 50% cell viability after exposure of cells for 44 hours at 10 μ M

^e less than 50% reduction of mean reporter signal